Short/Small Crack Model Development for Aircraft Structural Life Assessment

Min Liao [1*], Guillaume Renaud [1], Yan Bombardier [1]

[1] Aerospace Structures, National Research Council Canada (NRC)
1200 Montreal Rd, Ottawa, Ontario, Canada K1A 0R6
* Corresponding author: min.liao@nrc-cnrc.gc.ca

Abstract This paper presents the testing and modeling results from an NRC project on short/small [①] crack model development for aircraft structures. Fatigue tests were conducted for 7075-T73 hand forging aluminium material using precracked compact tension (C(T)) and naturally cracked single edge-notch tension (SENT) coupons, under various stress ratios. The adjusted compliance ratio (ACR) method was used for the C(T) coupon tests aiming to quantify remote closure due to plasticity and forging-induced residual stresses. For the SENT coupons, three-dimensional StressCheck finite element (FE) models were developed to accurately calculate the stress intensity factors of surface and corner cracks. Both C(T) and SENT test data were combined to develop short-long fatigue crack growth rate models. These models were then used in crack growth life analyses for coupon and component cases, taken from transport aircraft under spectrum loadings. It was shown that the newly developed models resulted in more accurate fatigue life estimations.

Keywords Short/small crack growth, 7075-T73 , Adjusted compliance ratio, Marker bands, CanGROW.

1. Introduction

Currently, the practical life prediction technologies for metallic aircraft structures are mainly safe-life (SL), damage-tolerance (DT, including fail-safe), and flaw-tolerance (including flaw-tolerance safe-life for helicopter). In addition, a combined SL and DT (two-stage) total life approach is used to overcome the limitations of these two approaches taken separately. However, the transition between SL and DT is not clearly defined and justified. One of the reasons is that the small crack region remains a "grey zone" for which a robust/practical approach and test database are still missing for many aircraft designers/manufacturers, although extensive research has been carried out in the past decades. In collaboration with other organizations, NRC is developing the Holistic Structural Integrity Process (HOLSIP) to augment the traditional SL and DT approaches with the ultimate goal to evolve HOLSIP into a new paradigm for both the design and sustainment stages. One of the current HOLSIP development efforts is to further develop the short/small crack database and the physics-based models.

Recently, an NRC project was completed with testing and modeling results for 7075-T73 aluminum forging material, which is used in Royal Canadian Air Force (RCAF) large transport aircraft [1]. A literature review revealed that short/small crack data are scarce for 7075-T73 aluminum alloys for fatigue durability analysis of aircraft structures. The short/small crack growth rate data have significant scatter due to material microstructures, specimen types and geometries, testing and measuring techniques, which lead to extensive testing time and costs. As such, some researchers perform long precrack crack tests and use the near-threshold data to represent the average small crack growth rate, which has two issues: 1) the long crack data produce overly high stress intensity threshold factor ΔK_{th} (ΔK at da/dN=3.94E-9 inch/cycle or 1E-10 m/cycle in ASTM E647) which would result in un-conservative life prediction; 2) the scatter is different from that of naturally small cracks, which are more affected by intrinsic microstructures effects.

[①] As per ATSM E647 (Appendix X3), a *small crack* is defined as being small when all physical dimensions (in particular, both length and depth of a surface crack) are small in comparison to a relevant microstructural scale, continuum mechanics scale, or physical size scale. While a *short crack* is defined as being short when only one physical dimension (typically, the length of a through-crack) is small according to the description of '*small crack*'.

For the long crack tests, the Adjusted Compliance Ratio (ACR) method [2] was proposed to adjust the stress intensity factor range (ΔK) by considering the remote crack closure effect, and then result in a lower threshold ΔK_{th}. Also the ACR method was able to quantify bulk residual stress in the remote closure, and then reduced the scatter and bias related to residual stress and sampling effects [3]. Efforts were also carried out on improving the ASTM E647 load reduction (LR) method, which is suspected to result in improper loading history effects on crack closure. These efforts include the compression precracking (CP) procedures [4], which also result in lower ΔK_{th} values.

For naturally nucleating small crack, the ASTM E647 (Appendix X3) introduces several experimental techniques, which are useful for measuring the growth of fatigue cracks sized on the order of 50μm or greater, and some are applicable to even smaller cracks. For small surface crack measurements, the silicon-based replication technique is at least as reliable as the traditional acetate-based replication, and it has no apparent effect on the fatigue life of the specimen. For small crack depth measurement, NRC has gained extensive experience in the use of the marker band (MB) technique to measure small crack profile on a fracture surface in a previous project.

Considering all the above factors, it was decided to test the 7075-T73 hand forging material, using both compact tension (C(T)) coupons with ACR method and single edge-notch tension (SENT) coupons with MB and replication techniques.

2. Short/small crack tests

The 7075-T73 hand forgings were made following the AMS-QQ-367 specifications. NRC received four forging blocks that were 2.0" thick, 2.5~3.5" wide, and 30"~72" long. A microstructural analysis showed that this alloy has more and larger particles than pores on the ST plane (short-transverse, the crack plane), and that the particle sizes range roughly from a few μm to 20-30μm. The grain sizes on the ST plane can reach 100μm. The tests were performed under laboratory environment; room temperature, 24 ± 3ºC and relative humidity, 30 ± 25%. The X-ray diffraction measurements, on 10 sampling spots, showed that surface residual stresses were scattered from -4 to +5 ksi (-28~34 MPa), with an average residual stress of 0.5 ksi (3.4 MPa).

2.1. Fatigue crack growth tests using C(T) coupons

A compact tension C(T) coupon was designed based on ASTM E647. The width of the coupon was 2.0" (5.08 mm) and the thickness was 0.25" (6.35mm). Each coupon was tested through precracking, *K*-decreasing, *K*-increasing, and constant loading following the E647 procedures. Six stress ratios (R=0.05, 0.33, 0.45, 0.60, and 0.80), were tested using a loading frequency of 5-10 Hz. The ACR method, developed by Fatigue Technology Associate (FTA), was used to estimate the effects of the remote crack closure, which refers to crack tip shielding as a result of contact in the crack wake behind the crack tip. This is in contrast to other shielding mechanisms near to the crack tip such as plasticity. The ACR method is based on the same measurement signals that are used for the 2% crack opening force method in E647 (Appendix X2), but it does demand high quality signals with less noise. The ACR stress intensity factor, ΔK_{ACR}, is calculated as described in Figure 1.

In addition to the ΔK_{ACR} results, the FTA software also provides two additional methods to estimate the effective stress intensity factor ranges (ΔK_{eff}) [②], i.e. the ASTM 2% opening load method ($\Delta K_{eff\text{-}OP}$) and the 2/π method ($\Delta K_{eff\text{-}2/\pi}$, partial closure correction below the opening load). Results

[②] Although the effective stress intensity factor range is a useful parameter, it should be noted that different definitions and calculations have been used in different applications. They may not be comparable to each other.

comparing these methods are provided in Figure 2 for an example coupon (No. H2, R=0.6). This figure shows large differences between the ΔK_{App} ($\Delta K_{eff\text{-}ACR}$ in the figure) and other ΔK_{eff} results at the near-threshold region. The $\Delta K_{eff\text{-}2/\pi}$ results are close to the ΔK_{ACR} whereas the $\Delta K_{eff\text{-}OP}$ results are lower than others, and the $\Delta K_{eff\text{-}OP}$ method is deemed to over-compensate the near-threshold data.

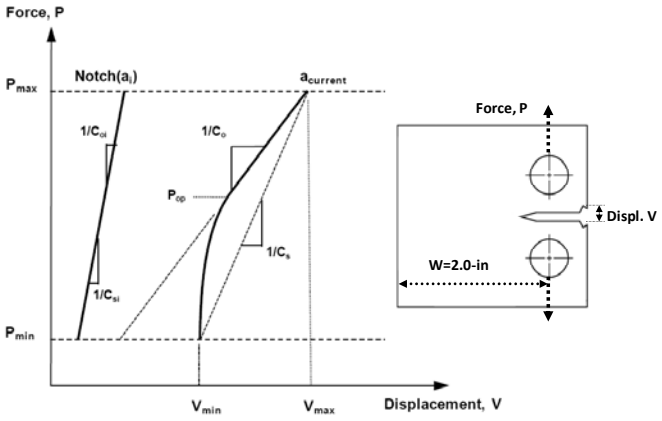

$$\Delta K_{ACR} = U_{ACR}\,\Delta K_{App}$$

$$U_{ACR} = \frac{C_{0i}}{C_{si}}\frac{C_s - C_{0i}}{C_0 - C_{0i}}$$

- ΔK_{App} is the full range, applied stress-intensity factor
- C_{oi}/C_{si} compensates for a possible bias in the secant or open-crack compliances because of signal conditioning noise or nonlinearity

Figure 1. Schematic of force-displacement curve showing critical parameters for ACR method (based on [2])

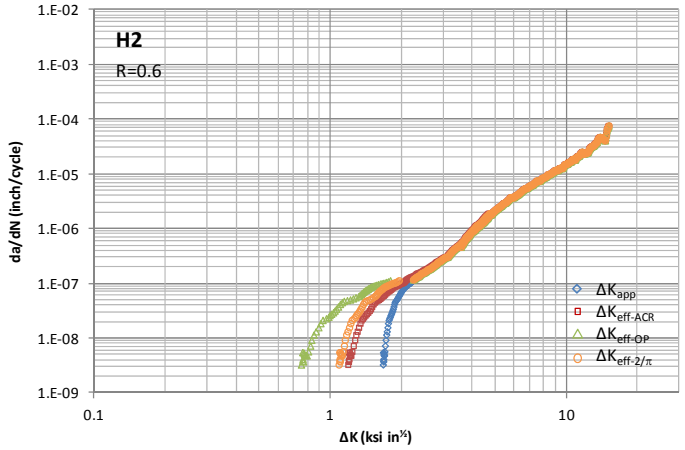

Figure 2. Typical crack growth rate results (coupon H2, R=0.60) (1-in=25.4 mm, 1.0 ksi√in=1.1 MPa√m)

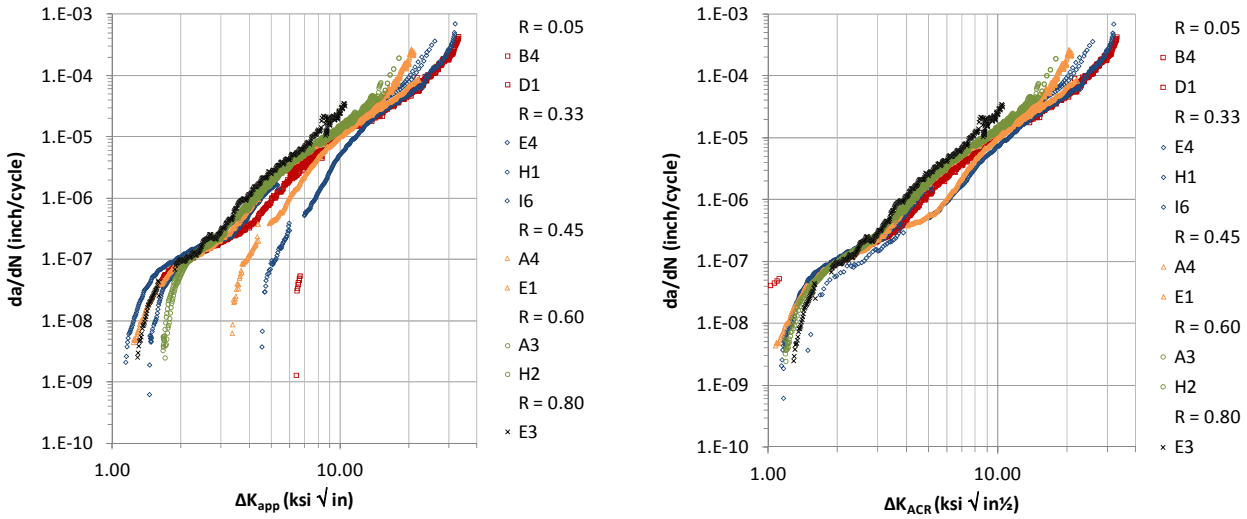

(a) da/dN-ΔK_{App} (before ACR correction) (b) da/dN-ΔK_{ACR} (after ACR correction)

Figure 3. C(T) test results at R=0.05,0.33,0.45,0.60,0.80 (1-in=25.4 mm, 1.0 ksi√in=1.1 MPa√m)

The C(T) test results for all *R*-ratios are presented in Figure 3: (a) da/dN-ΔK_{App} (before ACR correction); and (b) da/dN-ΔK_{ACR} (after ACR correction). The comparison shows that the ACR method reduced the data scatter especially the "fanning" effect at the near-threshold region, and gave lower ΔK_{th} values by removing the closure and residual stress effects. The scatter reduction is in the low stress ratios (*R*0.05-0.45) than in the high stress ratios (*R*0.6-0.8). It is also noted that some ACR corrections are very small possibly due to the positive residual stress effects.

2.2. Small crack tests using SENT coupons

A SENT coupon, as shown in Figure 4-(a), was used for fatigue tests with naturally nucleating small surface cracks. A test matrix, shown in Figure 4-(b), was designed using a simple center composite circumscribe (CCC) design of experiment (DOE) method aiming to provide a complete set of data under six stress ratios (R) and five stress levels. The test loading spectra were constant amplitude loading with marker band (MB) loading sequences. The silicon-based replication technique (RepliSet^{TM}) was used to measure the surface crack length, and marker bands (MB) on the fracture surfaces were reconstructed to determine the crack depth.

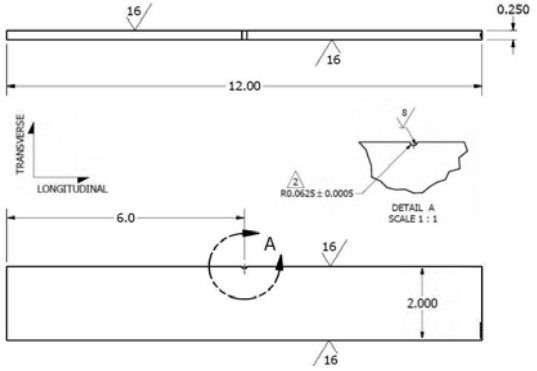

(a) SENT coupon (dimensions in inches, 1in=25.4mm)

Group No.	Replicate	Applied Max. Stress (ksi)	Applied Min. Stress (ksi)	Stress Ratio (R)
1	6	23.00	1.15	0.05
2	3	20.00	-6.00	-0.30
3	3	26.00	-7.80	-0.30
4	3	20.00	10.00	0.50
5	3	26.00	13.00	0.50
6	3	18.76	0.94	0.05
7	3	27.24	1.36	0.05
8	3	23.00	-23.00	-1.00
9	3	23.00	18.40	0.80

(b) SENT test matrix (1ksi=6.89MPa)

Figure 4. SENT coupon and test matrix

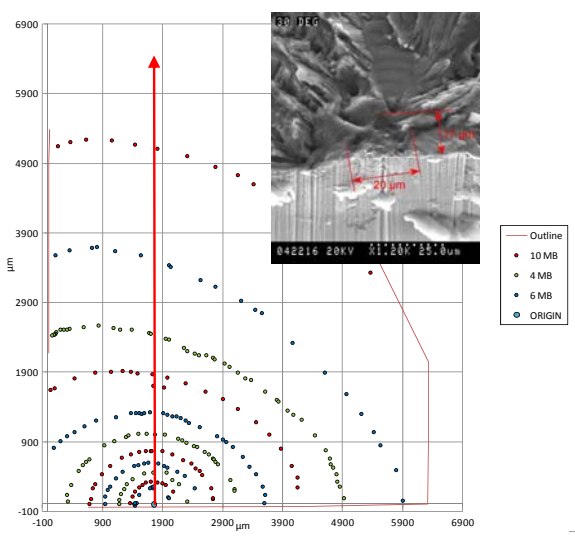

(a) single crack origin (pores)

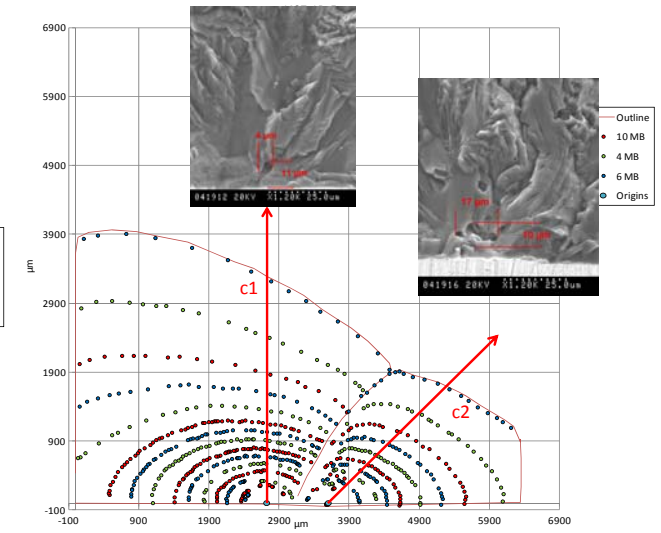

(b) multiple crack origins (pores/particles)

Figure 5. Typical SENT coupon marker bands and nucleation sites

The smallest replica crack detection was about 12 μm, and the smallest MB measured crack was about 20 μm. The MB crack detection resolution varied with stress levels and stress ratios, but

overall the MB technique could reliably provide 100 μm crack depth measurements. Fractography showed that cracks nucleated from 1) surface scratches; 2) particles or pores; and possibly 3) intragranular cracking. Many of these naturally nucleated cracks showed fairly rough fracture surfaces. Both corner and bore surface cracks, single and multiple were observed in various SENT coupons, as shown in Figure 5-b).

In general, the small crack growth rate data showed large scatter bands and irregular 'zigzag' (acceleration/deceleration) growth. The irregular growth rate was mainly due to microstructure effects (such as grain size, orientation, and grain boundary) associated with the scattered residual stresses, and secondarily caused by the measurement resolution/accuracy. More data analysis showed that the absolute measurement error (~5 μm) of the replication technique contributed only partially to the scatter band. Overall, the irregular 'zigzag' features were largely reduced after the crack size was over ~100 μm or dc/dN was about 3.94E-7 in/cycle (1E-8 m/cycle).

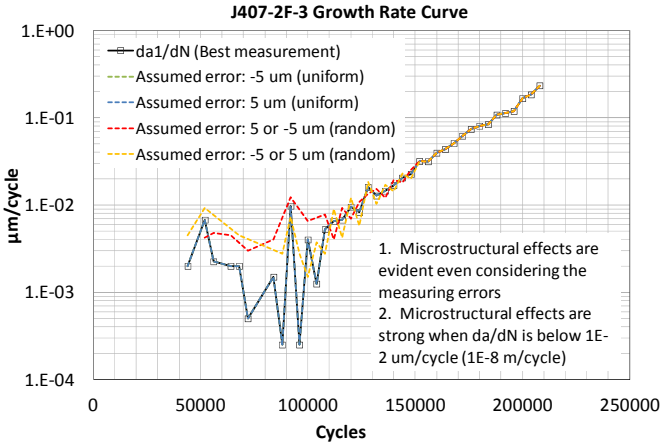

Figure 6. Typical surface small crack growth rate scatter (R= -0.3, σ_{MAX}= 20 ksi/138 MPa)

3. Small crack stress intensity factor modeling

A three-dimensional (3D) *p*-version StressCheck FE model was developed to calculate the stress intensity factors of the naturally nucleating cracks measured on the SENT test coupons [5]. The model was developed from a modified quarter-elliptical corner crack geometry at a hole. A useful feature of this model is that it was built as a parametric FE model, in which, as seen in Figure 7, various parameters can be assigned to the geometry of the crack, coupon, and mesh layers enclosing the crack front. Symmetry conditions can be assumed for surface crack modeling at a hole. The K-solutions were calculated at 96 points along the crack front, using the contour integral method with circular integration paths located between the first two concentric element layers. Eight elements were located along the crack front, with the extreme ones covering only the first and last 2 degrees to capture the peak stress intensity factor values close to the free surfaces. The analysis was performed with 8th degree polynomials. The process was automated using an Excel-based Visual Basic for Applications (VBA) program that could automatically configure the model, launch the analysis, and retrieve output results for a series of crack measurements in a specimen.

Previous verification examples have shown that the improved NRC solutions, developed from the hole geometry version of the aforementioned model, are more accurate than the classical Newman-Raju solutions, and comparable to the Fawaz-Andersson results tabulated in AFGROW, which however do not cover cracks smaller than 10% of the plate thickness and do not include the surface crack case (which are now available in the NRC solutions) [5].

The modeling of the test coupons was performed with the developed VBA program using the metrology results and crack measurements specific to each coupon. Doing so, no interpolation among crack size and crack shape values was performed. The crack growth rates were calculated using the secant method. Both the da/dN-ΔK_a (thickness direction) and dc/dN-ΔK_c (width direction) data points were calculated. The calculated crack growth rate dc/dN vs. ΔK (or K_{max} if R is negative) results of the single crack cases are illustrated in Figure 8. The ΔK_a and ΔK_c values were calculated from the StressCheck model at Φ = 85° and Φ = 0° (surface crack) or Φ = 5° (corner crack), respectively. In this paper, only single crack data were used in the K calculation.

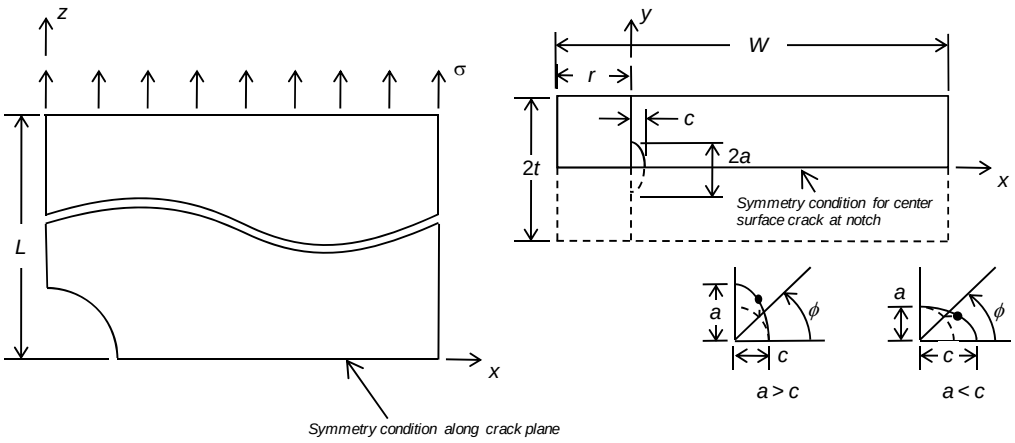

Figure 7. Definition of variables and boundary conditions

4. Comparison of precrack and natural small crack data (C(T) vs. SENT)

The crack growth rate data, generated from the C(T) tests (with and without ACR correction) and the SENT tests, are presented in Figure 8. The comparisons indicate that,

1) For long crack growth, da/dN>1E-7 in/cycle (2.54E-9 m/cycle), the C(T)-ACR and SENT test results are similar to each other, except for the R=0.05 case, which should include more crack closure than the high R-ratio cases. Without the ACR correction, some of the R=0.05 C(T) results were close to the SENT results, which had no ACR correction for the residual stress and closure effects. Meanwhile some other C(T) results showed negligible ACR correction, which involved very small residual stress, even tensile residual stress effects.
2) In the near-threshold region, da/dN<1E-7 in/cycle (2.54E-9 m/cycle), for R=0.05, the SENT results appear to give higher ΔK_{th} values than the C(T)-ACR results. The R=0.5 SENT tests did not provide enough data in the near-threshold region. But for R=0.8, the SENT results appear to give lower ΔK_{th} values than the C(T)-ACR results, for which the ACR correction is very small. Overall, the SENT results have more scatter than the C(T)-ACR results in the near-threshold region, and the SENT results should include less closure effect induced by small crack plasticity wake, but more machining-induced compressive residual stress on the surface layer (<50μm).

From the SENT and C(T) test results, a combined NRC short-long crack growth material model was developed as presented in Figure 9. The combined model is largely based on the SENT data, corrected with C(T)-ACR results to remove residual stress effect for R=0.05 and compensated with C(T)-ACR the near-threshold data for R=0.5. Note that the SENT data (ΔK) for R=-0.33 were shifted to the left using the ΔK ratio between the SENT and the C(T)-ACR long crack data for R=0.05, assuming the same residual stress effect in both tests. As a result, the NRC model is deemed to be a 'residual stress free' material model.

Some previous studies [1, 6] have indicated that, for the same 7xxx material, the plate and hand forging forms have the same composition, including particles and pores, but the grain aspect ratio and flow may be different near the surface. The hand forging shows more scatter in the crack growth rates; however, the average crack growth rates for both plate and forging are very similar to each other. Next, the developed NRC 'residual stress free' model, from the 7075-T73 forging tests, was used for fatigue life estimation of 7075-T73 plates.

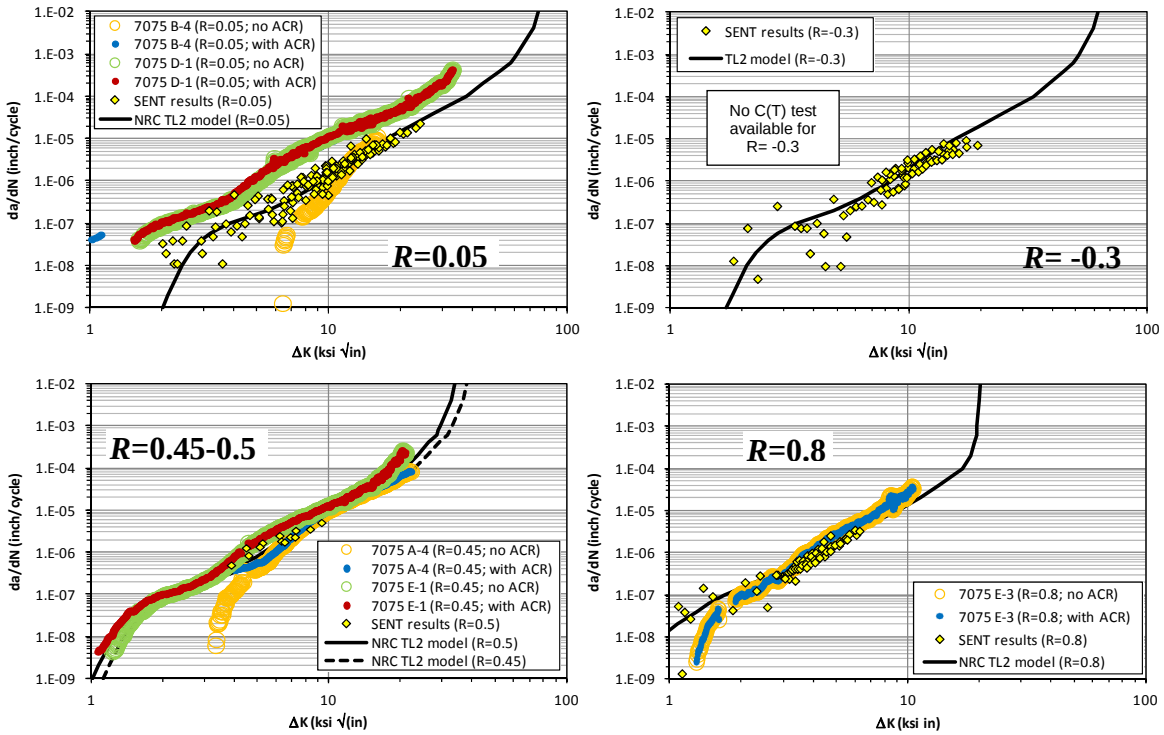

Figure 8. SENT and C(T) test results, and NRC (TL2) model for SENT (1-in=25.4 mm, 1.0 ksi√in=1.1 MPa√m)

da/dN(in/cycle)	*ΔK or K_{max}(ksi √in)*			
	***R* = 0.05**	***R* = -0.3**	***R* = 0.5**	***R* = 0.8**
1.E-09	1.42	1.20	1.01	0.71
2.E-09	1.49	1.27	1.07	0.77
1.E-08	1.69	1.46	1.25	0.92
2.E-08	1.83	1.60	1.40	1.08
4.E-08	2.04	1.79	1.61	1.30
6.E-08	2.25	1.98	1.78	1.45
1.E-07	2.66	2.33	2.09	1.69
2.E-07	3.90	3.39	2.97	2.29
4.E-07	4.98	4.37	3.92	3.16
6.E-07	5.73	5.04	4.53	3.70
8.E-07	6.31	5.56	5.02	4.13
1.E-06	6.69	5.91	5.36	4.45
2.E-06	7.93	7.01	6.40	5.36
4.E-06	9.45	8.38	7.67	6.49
1.E-05	12.28	11.00	10.29	9.12
2.E-05	15.34	13.76	12.87	11.39
4.E-05	19.38	17.23	15.84	13.52
1.E-04	26.58	23.32	20.90	16.89
2.E-04	31.27	27.15	23.81	18.38
4.E-04	36.56	31.21	26.44	18.97
6.E-04	40.52	34.23	28.38	19.45
8.E-04	41.83	35.18	28.92	19.46
1.E-03	43.14	36.18	29.55	19.61
4.E-03	50.34	41.46	32.65	20.04
1.E-02	52.96	43.39	33.80	20.28

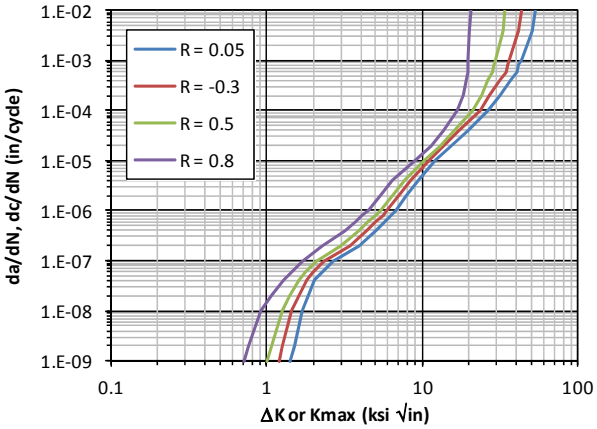

Figure 9. NRC combined material model for 7075-T73 (1-in=25.4 mm, 1.0 ksi√in=1.1 MPa√m)

5. Fatigue crack growth life estimation

5.1. Coupon life estimation

The NRC material model was used to estimate the crack growth lives of some 7075-T7351 plate

coupon tests under transport spectra [7], using the NRC in-house crack growth code CanGROW [9]. At first, a legacy material model of 7075-T7351 (Figure 10-(a)), based on the Forman equation, was used in association with the Hsu retardation model [8] using the default parameter value of $M_0 = 0.6$ and $R_{cut} = 0.3$. Both M_0 and R_{cut} are fitting parameters, and $M_0 = 1.0$, $R_{cut} = 0.0$ would create the most possible retardation and the longest life. As shown in Figure 10-(b), the fatigue life estimation using the legacy model were considered overly conservative, even when maximizing the Hsu retardation and considering that the legacy model was developed for a relative humidity of 90%. As shown in Figure 10-(b), using NRC Forman model converted from the R=0.5 curve in Figure 9, the life estimation was greatly improved, especially with the Hsu parameters calibrated at $M_0 = 0.2$ and $R_{cut} = 1.0$. Note that the spectrum was counted using the rainflow method in the above analyses.

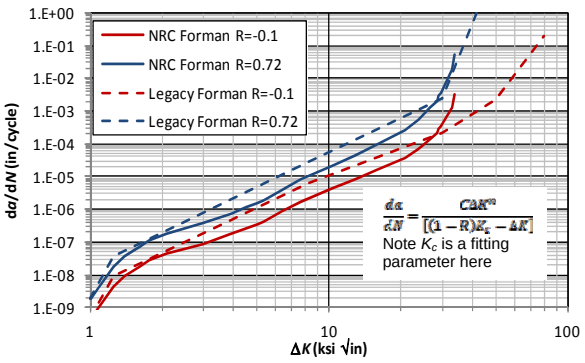

(a) 7075-T73 material model, legacy and NRC

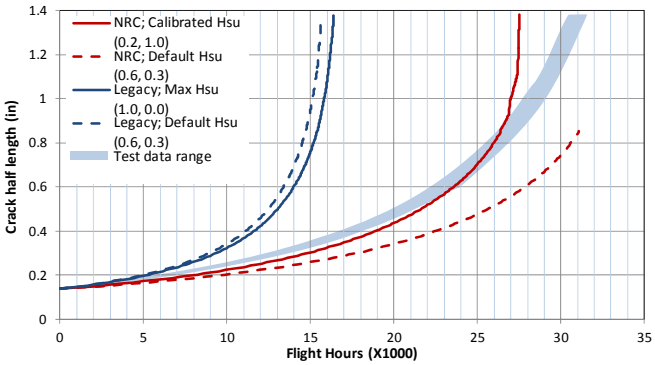

(b) Coupon life estimation using legacy and NRC models

Figure 10. Coupon life estimation using CanGROW (1-in=25.4 mm, 1.0 ksi√in=1.1 MPa√m)

It was also noted that one weakness of the Forman equation is lack of flexibility to correctly describe and shift the da/dN-ΔK curves between different stress ratios (R), because the shifting solely depends on a fitting parameter (K_C) that controls the K-factor near the fracture region. The mismatched shifting was also reported at the low-ΔK region [11]. Using the tabular data in Figure 9 should avoid this issue. In another preliminary study, the NRC model at R=0.8 was simply used as a ΔK_{eff} baseline model in FASTRAN3.8 for the coupon life estimation. As shown in Figure 11-(b), good agreement was achieved between the FASTRAN analysis and tests. Two previous 7075-T73 material models from [4,10] were also compared to the NRC model in Figure 11-(a), which resulted in one poor (blue, before calibration) and one good (yellow after calibrating) life estimations. The FASTRAN analysis used a crack closure model with more parameters (e.g. constraint factors), which calibrating details are beyond the scope of this paper. Note that the spectrum was used in the FASTRAN analysis without a cycle counting process.

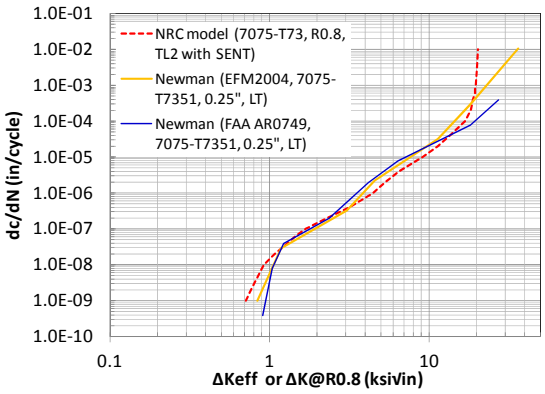

(a) 7075-T73 material models

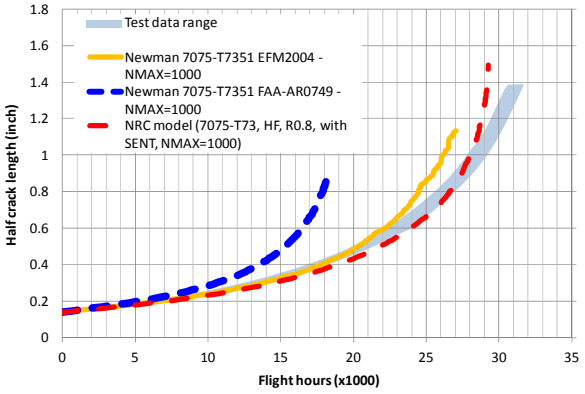

(b) Coupon life estimation

Figure 11. Coupon life estimation using FASTRAN (1-in=25.4 mm, 1.0 ksi√in=1.1 MPa√m)

5.2. Damage tolerance analysis of an aircraft component

A damage tolerance analysis (DTA) was carried out for the CW-1 critical location of the CC-130 center wing, made of 7075-T7351 plate, illustrated by the sketch in Figure 12. Since the DTA involves a multiple, phase-by-phase (PBP) crack growth analysis, the NRC in-house tool CanGROW was originally developed for such PBP analysis purpose. Prior to calibrating the CC-130 strain gauge based spectrum, the Hsu retardation model with default parameters was used in the DTA. Again, both the legacy and NRC Forman material models were used for the DTA, and the results are presented in Figure 12-(b). The legacy material model resulted in a fatigue life that was 45% shorter than that of NRC material model.

Because multiple site fatigue damage (MSD) was found in-service, the PBP analysis was updated by an MSD analysis, as shown in Figure 13. Using the unique MSD analysis module developed in CanGROW, the legacy material model provided an MSD crack growth life approximately 40% of the NRC material model. However, the MSD life to the critical crack size of 6.2 inches (157 mm) was about 17% less than the PBP life. Currently, these DTA results are considered as preliminary until a component test is available to validate these analyses.

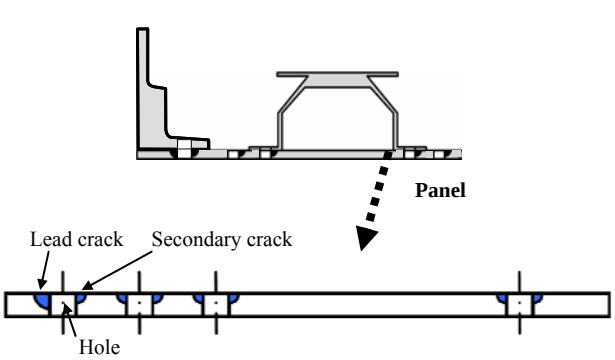

(a) PBP initial cracking model

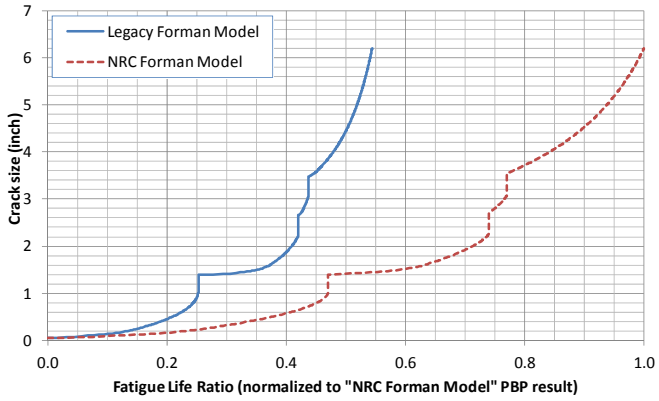

(b) Crack size vs. fatigue life

Figure 12. PBP DTA using CanGROW and CC-130 strain gauge spectrum (1-in=25.4 mm)

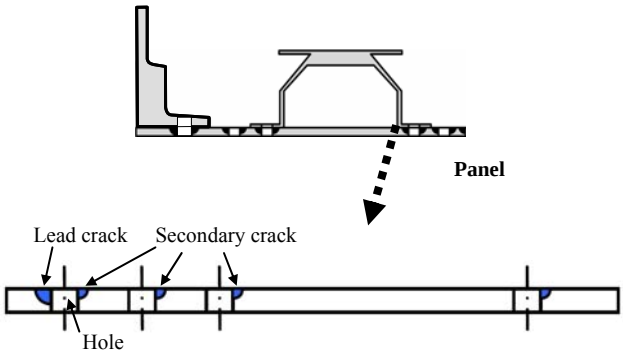

(a) MSD initial cracking model

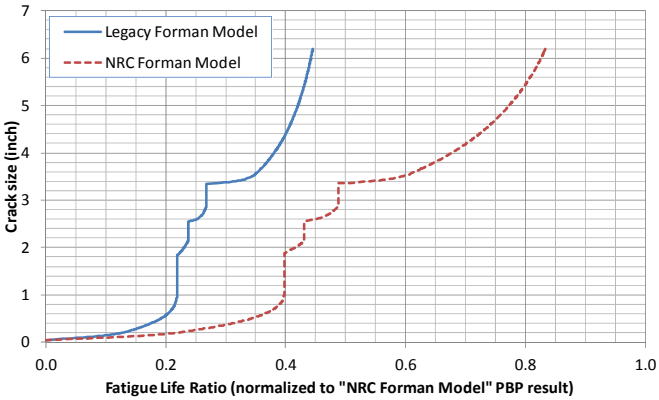

(b) Lead crack size vs. fatigue life

Figure 13. MSD DTA using CanGROW and CC-130 strain gauge spectrum (1-in=25.4 mm)

6. Conclusions

Both precracked long crack test (C(T)) and natural small crack test (SENT) have been carried out to generate short-long crack data under various stress ratios. The ACR method, coupled with the ASTM E647 load reduction method, reduced the scatter of crack growth rate data caused by the

closure and residual stress effects, especially under the low *R*-ratios but not under the high *R*-ratios. The natural small crack growth rate data showed that the "fanning" effect at the near-threshold region is mainly due to the material microstructural scatter, which cannot be determined by long crack tests. Both silicon-based replication and marker band techniques offered very good crack detection resolutions.

The C(T) and SENT data were then combined to develop an NRC material short-long crack model for 7075-T73 aluminum alloys. Using this model and the NRC in-house crack growth tool CanGROW, a good life estimation was achieved for coupon tests under transport loading spectra. Shortcomings were found for a legacy model that includes the Forman equation and Hsu retardation in the spectrum load life analysis. The CC-130 component case showed the difference in the DTA analyses using the legacy and NRC material models, for both PBP and MSD scenarios. Component test data are needed to further validate the DTA analyses and their differences. Tests cases on total fatigue life estimation are also needed to further validate the developed small crack material model.

Acknowledgements

This work was carried out with the financial support of Defence Research and Development Canada and NRC, Projects ''Short Crack Model Development for Helicopter Structural Life Assessment" and "Integrated Structural Life Assessment Method for the CF Air Fleets". Thanks to Defense Science and Technology Organization (DSTO) of Australia for providing some coupon test results.

References

[1] M. Liao, G. Renaud, Y. Bombardier, R. Desnoyers, T. Benak, Short crack model development for aircraft structural life assessment – final report, LTR-SMPL-2011-0239, Sept. 2011.

[2] J.K. Donald, G.H. Bray, R.W. Bush, An Evaluation of the Adjusted Compliance Ratio Technique for Determining the Effective Stress Intensity Factor, 29th National Symposium on Fatigue and Fracture Mechanics, ASTM STP 1332, T. L. Panontin, S. D. Sheppard, Eds., American Society for Testing and Materials 1998.

[3] D.L. Ball, J.K. Donald, M.A. James, and R.J. Bucci, The relationships between crack closure, specimen compliance and 'effective' fatigue crack growth rate, Proceedings of the 2011 ICAF, Montréal, June 1-3, 2011 (pp.265-276).

[4] J.C. Newman, Jr., Analyses of Fatigue Crack Growth Databases for Use in a Damage Tolerance Approach for Aircraft Propellers and Rotorcraft, DOT/FAA/AR-07/49, 2007.

[5] G. Renaud, M. Liao, Y. Bombardier, Improved stress intensity factor solutions for surface and corner cracks at a hole, 53rd AIAA/ASME/ASCE/AHS/ASC Structures, Structural Dynamics and Materials Conference, April 2012, Honolulu, Hawaii.

[6] R.W. Bush, R.J. Bucci, P. E. Magnusen, and G.W. Kuhlman, Fatigue crack growth rate measurements in aluminum alloy forgings: effects of residual stress and grain flow, Fracture Mechanics: 23rd Symposium. ASTM STP 1189. R. Chona, Ed., ASTM, 1993, pp.568-589.

[7] R. Ogden, D. Hartley, L. Meadows, Determination of the RAAF C-130J-30 Hercules wing Structural life of type through full scale fatigue testing, 2011 ASIP Conference, San Antonio.

[8] T. Deiter, Hsu model, AFRL-RB-WP-TR-2008-3, 2004.

[9] Y. Bombardier, M. Liao, G. Renaud, A new crack growth analysis tool for the assessment of multiple site fatigue damage, Proceedings of the 2010 Aircraft Airworthiness & Sustainment Conference, Austin, USA, 2010.

[10] J.C. Newman, A. Brot, and C. Matias, Crack-growth calculations in 7075-T7351 aluminum alloy under various load spectra using an improved crack-closure model, *Engineering Fracture Mechanics*, 71 (2004) 2347–2363.

[11] R.L. Circle, F.M. Conley, A Quantitative Assessment of the Variables Involved in Crack Propagation Analysis for In-service Aircraft, *J. of Aircraft*, 18 (1980) 562-569.